LIMNOLOGY and OCEANOGRAPHY

ASLO

Limnol. Oceanogr. 9999, 2023, 1–15

doi: 10.1002/lno.12410

Phytoplankton community response to episodic wet and dry aerosol deposition in the subtropical North Atlantic

Zhongwei Yuan [1,2] **Eric P. Achterberg** [1] **Anja Engel** [1] **Zuozhu Wen** [1,2] **Linbin Zhou** [1,3] **Xunchi Zhu** [1,4] **Minhan Dai** [2] **Thomas J. Browning** [1*]

[1]Marine Biogeochemistry Division, GEOMAR Helmholtz Centre for Ocean Research, Kiel, Germany
[2]State Key Laboratory of Marine Environmental Science, College of Ocean and Earth Sciences, Xiamen University, Xiamen, China
[3]CAS Key Laboratory of Tropical Marine Bio-resources and Ecology, Guangdong Provincial Key Laboratory of Applied Marine Biology, South China Sea Institute of Oceanology, Chinese Academy of Sciences, Guangzhou, China
[4]State Key Laboratory of Marine Resource Utilization in South China Sea, Hainan University, Haikou, China

Abstract

Atmospheric aerosol deposition into the low latitude oligotrophic ocean is an important source of new nutrients for primary production. However, the resultant phytoplankton responses to aerosol deposition events, both in magnitude and changes in community composition, are poorly constrained. Here, we investigated this with 19 d of field and satellite observations for a site in the subtropical North Atlantic. During the observation period, surface dissolved aluminum concentrations alongside satellite-derived aerosol and precipitation data demonstrated the occurrence of both a dry deposition event associated with a dust storm and a wet deposition event associated with strong rainfall. The dry deposition event did not lead to any observable phytoplankton response, whereas the wet deposition event led to an approximate doubling of chlorophyll *a*, with *Prochlorococcus* becoming more dominant at the expense of *Synechococcus*. Bioassay experiments showed that phytoplankton were nitrogen limited, suggesting that the wet deposition event likely provided substantial aerosol-derived nitrogen, thereby alleviating the prevalent nutrient limitation and leading to the rapid observed phytoplankton response. These findings highlight the important role of wet deposition in driving rapid responses in both ocean productivity and phytoplankton community composition.

Atmospheric aerosol deposition into the surface ocean can impact marine phytoplankton growth by supplying both nutritious and toxic elements, with important consequences for oceanic carbon sequestration and, ultimately, climate (Duce et al. 1991; Jickells and Moore 2015; Hamilton et al. 2022). Assessing the impact of aerosol deposition on phytoplankton under different biogeochemical settings is thus a key part of understanding the Earth System and its response to anthropogenically induced changes (Guieu et al. 2014).

Direct assessments of the impact of aerosol deposition on phytoplankton have been made via on-deck aerosol addition experiments (Hamilton et al. 2022 and references therein; Yuan et al. 2023). Such experiments have demonstrated that while positive phytoplankton growth responses following artificial aerosol addition are common, negative impacts or limited responses have also been observed. This variability has highlighted the importance of both the specific aerosols and the biogeochemistry of the receiving seawater in determining the response of phytoplankton to aerosol deposition (Guieu et al. 2014; Martino et al. 2014; Hamilton et al. 2022).

Due to the highly episodic and geographically patchy nature of aerosol deposition, in situ field observations of their impacts on natural, unincubated phytoplankton communities, particularly in remote ocean areas, are a challenge. To address this, most studies have utilized satellite- and/or model-derived estimates of aerosol deposition and phytoplankton biomass (Bishop et al. 2002; Tang et al. 2021; Ardyna et al. 2022). Some studies have also accumulated evidence through assessment of in situ chlorophyll *a* (Chl *a*) in response to aerosol deposition events (DiTullio and Laws 1991;

*Correspondence: tbrowning@geomar.de

Additional Supporting Information may be found in the online version of this article.

Author Contribution Statement: Z.Y., T.J.B., and E.P.A. co-designed the study. Z.Y., T.J.B., E.P.A., A.E., Z.W., L.Z., X.Z., and M.D. contributed to data acquisition and analysis. Z.Y. and T.J.B. analyzed and interpreted the data and drafted the manuscript with contributions from all authors.

Kramer et al. 2020; Milinković et al. 2022). Although all of these studies emphasized the general patterns of increased phytoplankton biomass with elevated aerosol deposition, the causative link between them was not always clear. This is partly due to the potential impact of several environmental factors, including alternative nutrient supply routes, and changes in temperature, light availability, and mixed layer depth, which all potentially contribute to any changes in phytoplankton biomass alongside aerosol supply (Boyd et al. 2010; Mahadevan et al. 2012; Mignot et al. 2018).

Few studies have considered the importance of the aerosol deposition pathway, either through dust storms (dry deposition) or rainfall events (wet deposition; Ridame et al. 2014; Van Wambeke et al. 2021), despite them potentially differing in terms of aerosol acidity (lower pH under wet deposition) and settling efficiency in the air (elevated under wet deposition), which is expected to have a critical impact on the magnitude of nutrient supply (Baker et al. 2007, 2010; Jung et al. 2011). In addition, we know comparatively little about how aerosol deposition affects specific phytoplankton groups (DiTullio and Laws 1991; Kramer et al. 2020), despite this potentially having important implications for carbon export; for instance, phytoplankton blooms dominated by diatoms are more likely to trigger enhanced export of faster-sinking particulate organic carbon to the ocean interior (Martin et al. 2011; Leblanc et al. 2018).

The North Atlantic Subtropical Gyre (NASG) is characterized by the depletion of both dissolved inorganic nitrogen and phosphate, which constrains phytoplankton growth (Marañón 2005; Moore et al. 2013). Aerosol deposition of these deficient nutrients, primarily nitrogen (N) and to a lesser extent phosphorus (P), could potentially stimulate primary productivity by alleviating these limitations (Baker et al. 2010; Zamora et al. 2013). In addition, aerosol deposition can also provide iron (Fe), which can be (co-)limiting to diazotrophs (N_2-fixing microbes) in this system, in turn contributing to an input of N into the system and enhancing primary productivity (Mills et al. 2004; Moore et al. 2009; Schlosser et al. 2014). However, aerosols in this region have been shown to have multiple potential sources, including the Sahara Desert, Continental Europe, North America, or from the remote ocean, which could result in strong differences in their chemical composition and thereby effectiveness as a nutrient supply mechanism (Baker et al. 2006; Patey et al. 2015). Collectively, differences in deposition magnitude, pathway, and the biogeochemistry of the receiving seawater complicate accurate prediction of phytoplankton response to aerosol deposition.

In this study, we present direct evidence on how pulsed aerosol inputs affect phytoplankton in the subtropical North Atlantic, by carrying out a detailed field investigation of the temporal variability of aerosol depositions, water column physics and biogeochemistry, and changes in phytoplankton biomass and community composition.

Methods

Study location and sampling

Sample collection and experiments were conducted on the RV Meteor cruise M176/2, a GEOTRACES process study, in the period from 01 September 2021 to 06 October 2021 in the NASG. Samples for vertical profiles were collected daily over 19 consecutive days (only Chl *a* samples were measured on 23 September 2021), using 24 × 12-liter trace-metal-clean Niskin-X bottles (Ocean Test Equipment) on a titanium conductivity-temperature-depth rosette frame. Surface seawater for the bioassay experiments was collected using a custom-built towed-fish located at 2–3 m depth, fitted with acid-washed tubing, with suction provided by an acid-washed Teflon bellows pump (Dellmeco A15). All samples were collected in a dedicated clean-air laboratory container with positive air pressure maintained via inward airflow passed through a high-efficiency particulate air filter. Mixed layer depth (MLD) was calculated as the depth of the 0.2°C temperature difference relative to a reference temperature at 10 m depth (de Boyer Montégut et al. 2004).

Macronutrient concentrations

Macronutrient samples for nitrate plus nitrite (hereafter simply referred to as nitrate) and phosphate were collected in duplicate in 15-mL acid-washed polypropylene tubes. One of the aliquots was analyzed on board using a segmented flow injection nutrient autoanalyzer (QuAAtro, Seal Analytical) and was checked against certified reference material distributed by KANSO Technos, Japan. The detection limits for this standard method were nitrate $= 0.033\ \mu mol\ L^{-1}$ and phosphate $= 0.005\ \mu mol\ L^{-1}$. The other aliquots were frozen immediately at −20°C and analyzed upon return to a land-based laboratory using a low-level method with a custom-assembled system with an analyzer (QuAAtro, Seal Analytical) equipped with 2 m waveguides (World Precision Instruments Inc.) as described by Patey et al. (2008). Detection limits for this low-level method were nitrate $= 7\ nmol\ L^{-1}$ and phosphate $= 3\ nmol\ L^{-1}$. The low-level method was employed for those samples whose concentrations were initially identified as being below $0.1\ \mu mol\ L^{-1}$ for either nitrate or phosphate via the standard method.

Dissolved trace metal concentrations

Dissolved trace metal samples were collected through a 0.8-/0.2-μm filter capsule (AcroPak, Pall) into 125-mL acid-clean Nalgene low-density polyethylene bottles and acidified to pH 1.9 with ultrapure hydrochloric acid (UpA, Romil). Concentrations of dissolved Fe (DFe) and dissolved copper (DCu) were analyzed following preconcentration on a SeaFAST device using inductively coupled plasma mass spectrometry (ICP-MS; Element XR, Thermo Scientific), with quantification via isotope dilution (Rapp et al. 2017). Certified reference seawater materials GSP (2009 GEOTRACES Pacific surface seawater) and GSC (2009 GEOTRACES coastal surface seawater)

were routinely analyzed alongside seawater samples, with GSP producing concentrations of 0.178 ± 0.035 nmol L^{-1} DFe and 0.580 ± 0.037 nmol L^{-1} DCu (mean ± SD, $n = 28$), and GSC producing concentrations of 1.522 ± 0.135 nmol L^{-1} DFe and 1.099 ± 0.149 nmol L^{-1} DCu (mean ± SD, $n = 38$), which agree with the consensus values (https://www.geotraces.org/standards-and-reference-materials/).

Concentrations of dissolved aluminum (DAl) were measured using a modified Al-lumogallion complex method following Ren et al. (2001). Briefly, 5 μL *o*-phenanthroline solution (16 mmol L^{-1}) and 30 μL Be^{2+} solution (50 mmol L^{-1}) were added to 10 mL seawater samples to remove the interferences from Fe and fluorine in seawater. The samples were buffered with ammonium acetate (2 mol L^{-1}; prepared by dissolving 11 mL acetic acid [UpA, Romil] and 15 mL NH_4OH (Optima grade) in deionized water [MilliQ, Millipore], and then diluted to 100 mL). Atlantic surface seawater (with a background DAl concentration of < 3 nmol L^{-1}) was used to prepare the solutions for the standard calibrations. The Al-lumogallion fluorescence was analyzed with a Carey Eclipse fluorometer (excitation wavelength 500 nm, emission wavelength 570 nm) and the detection limit of DAl was below 1 nmol L^{-1}.

Chl *a* concentrations

Samples for Chl *a* were filtered (100 mL) onto 25-mm diameter Fisher MF300 glass microfibre filter (GF/F) filters, extracted in the dark for 16–24 h in 10 mL 90% (by volume) acetone at −20°C, and analyzed on a precalibrated Turner Designs Trilogy laboratory fluorometer (Welschmeyer 1994). The concentrations of Chl *a* were used as an indicator of total phytoplankton biomass (implicitly assuming a constant carbon to Chl *a* ratio).

Diagnostic phytoplankton pigment concentrations

Samples for phytoplankton pigment analyses were filtered (4 liters) onto 25-mm diameter Fisher MF300 GF/F filters and frozen immediately at −80°C. Upon return to land, pigments were extracted in 90% acetone in plastic vials by homogenization of the filters using glass beads in a cell mill, centrifuged (10 min, 5200 rpm, 4°C), then the supernatant was filtered through 0.2-μm polytetrafluoroethylene filters (VMR International) and subsequently quantified by reverse-phase high-performance liquid chromatography (HPLC, Dionex UltiMate 3000 LC system, Thermo Scientific; Van Heukelem and Thomas 2001). Pigment standards were from Sigma-Aldrich and the International Agency for ^{14}C Determination. The analyzed pigments included Chl *a*, divinyl Chl *a*, Chl *b*, Chl c_2, Chl c_3, peridinin, 19′-butanoyloxyfucoxanthin, fucoxanthin, violaxanthin, 19′-hexanoyloxyfucoxanthin, diatoxanthin, alloxanthin, zeaxanthin, neox, α-carotene, and β-carotene. These pigment assemblages were used to associate the fractions of 11 phytoplankton groups to the total Chl *a* (TChl *a*, the sum of Chl *a* and divinyl Chl *a*) via CHEMTAX using published field-derived starting pigment ratios (Mackey et al. 1996; Veldhuis and Kraay 2004). These phytoplankton groups were diatoms, dinoflagellates, *Synechococcus*, high-light (HL) and low-light (LL) subpopulations of *Prochlorococcus*, prymnesiophytes type4 (T4), chrysophytes, prasinophytes, cryptophytes, *Trichodesmium*, and chlorophytes.

Flow cytometry

Flow cytometry samples (2 mL) were fixed with paraformaldehyde at a 1% final concentration (methanol-free 16% 10-mL glass ampules, Alfa Aesar/Thermo Fisher), mixed with a vortex, left for 10 min at room temperature in the dark, and then directly frozen at −80°C. Samples were analyzed upon return to shore using a FACSCalibur flow cytometer (Becton Dickenson). Cell counts were carried out in CellQuest software (Becton Dickenson). Plots of orange fluorescence vs. red fluorescence were used to identify and enumerate *Synechococcus* from other picophytoplankton, and plots of side scatter vs. red fluorescence (with *Synechococcus* gated out) were used to enumerate *Prochlorococcus*.

Bioassay experiments

Three nutrient amendment bioassay experiments were conducted, with seawater collection and experiment initiation on the 17 September 2021, 18 September 2021, and 26 September 2021, respectively. Experiments directly followed previously published protocols (Browning et al. 2017). Seawater was collected with the towed-fish around local midnight in 1-liter trace-metal-clean Nalgene polycarbonate bottles. One bottle was sampled immediately for initial measurement of Chl *a* concentration, with the remaining bottled seawater samples spiked in triplicate with P, Fe, or P + Fe for ~ 24-h incubation (Experiments 1 and 3), and N, P, Fe, N + P, N + Fe, P + Fe, or N + P + Fe for ~ 50-h incubation (Experiment 2) along with non-nutrient-amended controls. Treated bottles were spiked to the following nutrient concentrations: $N = 1$ μmol L^{-1} $NaNO_3$ + 1 μmol L^{-1} NH_4Cl; $P = 0.2$ μmol L^{-1} NaH_2PO_4; and Fe = 2 nmol L^{-1} $FeCl_3$ (from a solution stabilized in 0.01 mol L^{-1} HCl). N and P treatment solutions were previously passed through a prepared Chelex 100 column to remove trace metal contaminations. Bottles were placed in an on-deck incubator flushed with continuously replenished surface waters from the ship's underway flow-through system to maintain temperatures. The incubator was screened with Blue Lagoon screening (Lee Filters), which maintained irradiance at ~ 30% of that of the surface ocean. Following the incubation period, bottles were subsampled for analysis of Chl *a*.

Satellite observations

Daily and monthly composites of 0.5° resolution Aqua Moderate Resolution Imaging Spectroradiometer (Aqua/MODIS) aerosol optical thickness (AOT) for September 2021 were downloaded from the NASA Earth Observations (https://neo.gsfc.nasa.gov/). Daily accumulated precipitation at 0.1°

resolution (Global Precipitation Measurement) was downloaded from GIOVANNI (https://giovanni.gsfc.nasa.gov/giovanni/). Daily sea-level anomaly (SLA) at 0.25° resolution was obtained from the Copernicus Marine Data Store (L4 product downloaded from: https://data.marine.copernicus.eu/). Daily satellite-derived Chl *a* at 4 km resolution was downloaded from the NASA Ocean Color website (standard Aqua/MODIS L3 product, https://oceancolor.gsfc.nasa.gov). Seven-day air mass backward trajectories were calculated from the NOAA's Air Resources Laboratory using the Hybrid Single-Particle Lagrangian Integrated Trajectory model (HYSPLIT) at the starting height level of 1000 m (https://www.ready.noaa.gov/hypub-bin/trajasrc.pl). The 7-d trajectory choice was a balance between long enough durations to clearly indicate potential source regions and the increasing uncertainty in trajectories with increasing time.

Calculation of daily dust deposition fluxes

Aluminum, a major component of eolian dust, is not readily depleted from surface waters as a result of its restricted uptake by microbes, and therefore is considered a quantitative tracer to constrain dust deposition fluxes (Measures and Brown 1996; Barraqueta et al. 2019; Benaltabet et al. 2022). In this study, the satellite-derived AOT and precipitation showed high consistency with the daily surface DAl concentrations (*see* Fig. 2f, Supporting Information S3, S4); we therefore used DAl to make approximate estimates of dust deposition fluxes via the Measurement of Aluminum for Dust Calculation in Open Waters (MADCOW) model (Measures and Brown 1996), shown in the following equation:

$$G = \frac{\mathrm{DAl} \times \mathrm{MLD}}{\tau \times \mathrm{S} \times \mathrm{D}} \quad (1)$$

where G is the total dust deposition flux (g m^{-2} yr^{-1}), DAl is the average concentration in the mixed layer, MLD is the depth of the mixed layer (m), τ is the Al residence time (yr), which is defined as the quotient between the total DAl inventory in the mixed layer and the rate of input or removal, S is the fractional solubility of Al in dust (%), and D is the concentration of Al in dust (8.1% by weight, equal to 3000 μmol g^{-1}). Previous studies have indicated that biological processes, including passive absorption onto biogenic particles and active biological uptake by diatoms, dominate the removal of DAl in the remote open ocean (Moran and Moore 1988; Middag et al. 2015), with negligible contributions from non-biogenic particles (< 10% of the total particles; Emerson et al. 1997). As a result, the residence time is inferred to be proportional to the biological productivity, which is closely tied to phytoplankton biomass (assumed proportional to Chl *a*).

Statistical analyses

All statistical analyses were performed in R 4.1.2 (R Development Core Team 2021) and particularly functions embedded in the "vegan" package (Oksanen et al. 2022). The dissimilarities in phytoplankton community structure were assessed with the Bray–Curtis dissimilarity index. Principal component analysis (PCA) was used to identify possible clusters. The contribution of different environmental factors to the PCA ordination plot was assessed using an envfit analysis (R function envfit used with 999 permutations, "vegan" package). The obtained coefficient of determination (R^2) gives the proportion of the main variability (i.e., the main dimensions of the ordination) that can be attributed to environmental factors.

Results

Study location conditions

The field sampling was performed at a daily frequency in the oligotrophic NASG within a study area of 30 × 37 km (Fig. 1a; Supporting Information Fig. S1), which we assume to be equivalent to a single location time-series observation. During the observation period, satellite-derived SLA indicated relatively modest eddy activity, with SLA increasing from ~ 8 to ~ 12 cm, reflecting persistent convergence of surface waters (Fig. 1b; Supporting Information Fig. S2). Although highest AOT over the study site occurred on 15 September and 17 September (Supporting Information Fig. S3), highest rainfall at the study site was observed on 23 September to 24 September, with a maximum precipitation rate of up to 61 mm d^{-1} (Fig. 1c; Supporting Information Fig. S4). The mean, shipboard-determined concentrations of Chl *a* in the mixed layer remained relatively stable until 23 September to 24 September, when a significant increase (0.20 ± 0.01 μg L^{-1}) was observed, approximately doubling the concentration seen in the preceding days (0.11 ± 0.01 μg L^{-1}, n = 14 d); this concentration then declined slightly to 0.17 ± 0.01 μg L^{-1} on 25 September to 27 September (n = 3 d; Fig. 1c). Although satellite coverage on 23 September to 24 September was poor, satellite-derived surface Chl *a* concentrations on 25 September also demonstrated a broad-scale increase around the study site (Supporting Information Fig. S5).

Physical and chemical parameters

Over the study period, the range of MLD varied between 19 and 40 m (Supporting Information Table S1). Water column profiles of temperature showed persistently strong vertical gradients, which decreased sharply from approximately 25°C at the surface to as low as 16°C at 120 m, with no clear temporal variation (Fig. 2a). In contrast, salinity exhibited much larger temporal fluctuations (Fig. 2b): a distinct decline in surface mixed layer salinity was observed to coincide with the episodic rainfall event on 24 September. The distribution of density was generally consistent with temperature (Fig. 2c). Concentrations of nitrate and phosphate were uniformly low in the mixed layer (1–68 nmol L^{-1} for nitrate and 4–27 nmol L^{-1} for phosphate; Fig. 2d,e) with no clear temporal trends. Vertical profiles of DAl showed distinct variations with

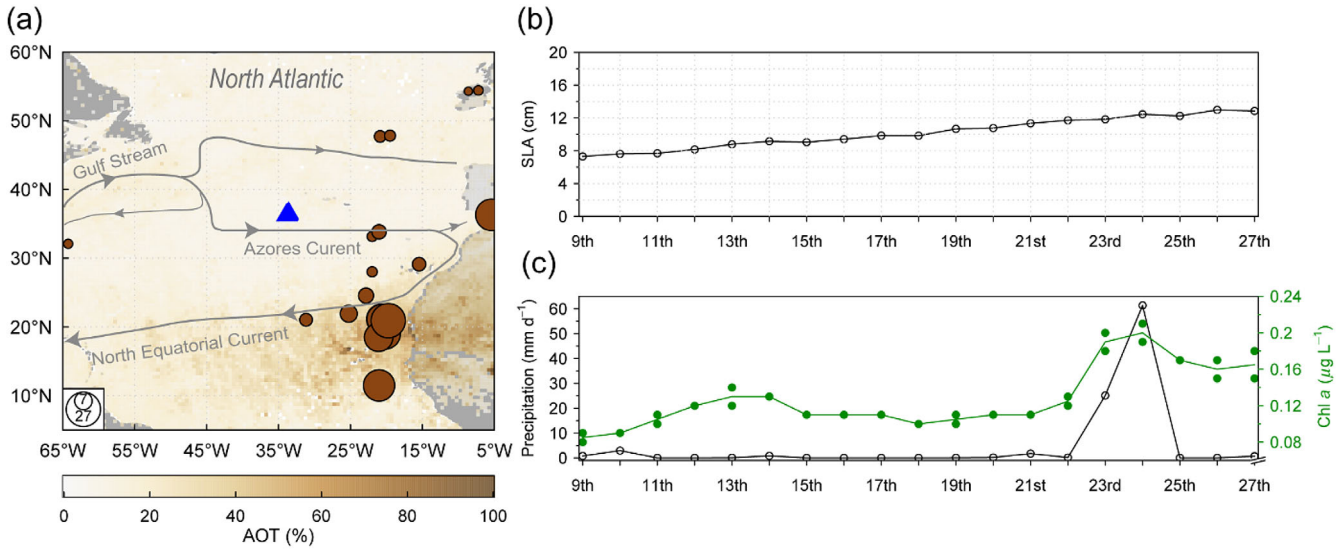

Fig. 1. Field sampling location and environmental conditions during the cruise. (**a**) Map of the North Atlantic showing the sampling station (blue triangle) on a background of September 2021 average AOT. Observed dust deposition fluxes from Albani et al. (2014) are shown as circles (g m^{-2} yr^{-1}). Gray lines indicate the main surface ocean currents (Talley et al. 2011). (**b**) Daily satellite-derived SLA at the study site during the sampling period. (**c**) Daily satellite-derived precipitation (black circles) and shipboard Chl *a* in the mixed layer (green dots = individual values; green line = mean values) at the study site during the sampling period.

depth (Fig. 2f). A minimum DAl concentration of ~ 7 nmol L^{-1} was consistently observed between 40 and 100 m depth, apart from samples collected on 16 September to 18 September, where elevated concentrations extended to the full depth profiles. This feature also coincided with enhanced atmospheric aerosol loading on 15 September and 17 September, as inferred from the satellite-derived AOT (Supporting Information Fig. S3). Surface DAl concentrations markedly increased (to ~ 15 nmol L^{-1}) starting from 24 September 24, consistent with the elevated precipitation rate on that day (Fig. 1c; Supporting Information Fig. S4). Likewise, the enhanced wet deposition also corresponded to increased surface DFe concentrations (Fig. 2g). However, across the dataset as a whole surface DFe and DAl were poorly correlated ($R^2 = 0.12$, $p = 0.154$). Vertical profiles of DCu showed a similar pattern to that of DFe, except during the wet deposition event when they were found to be decoupled, with no clear rise in surface DCu concentrations (Fig. 2h).

Estimated daily dust deposition fluxes

Given that the surface Chl *a* concentrations remained relatively constant before the episodic rainfall event (on average 0.11 ± 0.01 μg L^{-1}), we assumed that the residence time of Al during this period was identical to previously reported values, 5 yr (Measures and Brown 1996), with the remaining days linearly scaled to the corresponding surface Chl *a* concentrations (range of calculated residence times of 2.8–3.4 yr). Assuming the total fractional solubility of 6% in the study region (Baker et al. 2013), and in combination with the observed MLD and DAl, daily dust deposition fluxes using the MADCOW model were estimated to range between 0.5–3.0 mg m^{-2} d^{-1} (Supporting Information Table S1). Although this calculation is subject to significant uncertainties associated with residence time and fractional solubility (Measures and Brown 1996; Barraqueta et al. 2019), which will subsequently propagate to deposition flux estimates, this range is generally consistent with previous observations in the region (Fig. 1a; Albani et al. 2014) and results from other models (Han et al. 2008; Xu and Weber 2021). Notably, two significant increases in model-derived deposition fluxes were found on 17 September (1.6 mg m^{-2} d^{-1}) and on 24 September to 25 September (2.1 and 3.0 mg m^{-2} d^{-1}, respectively).

Phytoplankton community structure

The vertical distribution of TChl *a* was typical for the oligotrophic ocean, with a pronounced subsurface maximum ranging from 0.12 to 0.25 μg L^{-1} between 66 and 95 m depth. The average TChl *a* in the mixed layer remained fairly uniform across the observation period, with the exception of 24 September, where it increased 1.8-fold compared to average values (Figs. 3, 4; Supporting Information Fig. S6). This increase in TChl *a* was contributed largely by an increase in *Prochlorococcus* (HL subpopulation; contribution of 58% to the TChl *a* increase), followed by additional contributions from the other phytoplankton groups, including prymnesiophytes (27%), cryptophytes (16%), chrysophytes (13%), *Prochlorococcus* (LL subpopulation; 9%), and chlorophytes (3%), while

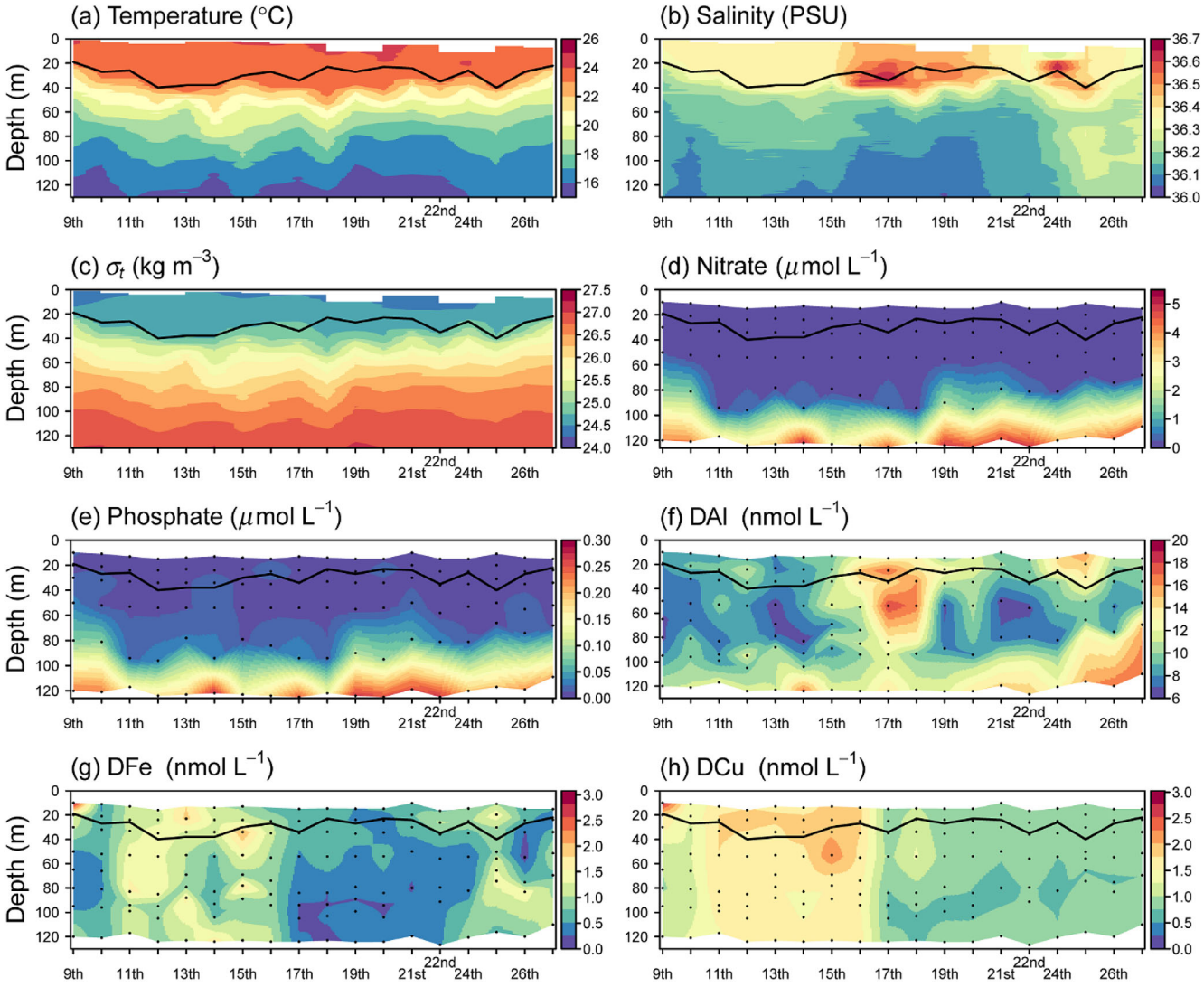

Fig. 2. Depth profiles of physical and chemical parameters. (**a**) Temperature, (**b**) salinity, (**c**) potential density anomaly (σ_t), (**d**) nitrate, (**e**) phosphate, (**f**) DAI, (**g**) DFe, and (**h**) DCu. Dots show sampling depths on each day, and black solid lines indicate the mixed layer depth. Data on 23 September 2021 were not collected.

Synechococcus reduced (−22% relative to the TChl *a* increase). The increased dominance of *Prochlorococcus* over *Synechococcus* inferred from the pigment analysis was independently supported by the sharp increases in their cell abundance ratios, as determined by flow cytometry analysis (Fig. 3a). In addition to the variabilities in total biomass, vertical differences in community composition were also observed. *Prochlorococcus* (HL subpopulation), *Synechococcus*, and prymnesiophytes collectively dominated the phytoplankton community in terms of chlorophyll biomass in the surface (accounting for > 70% of the TChl *a*), apart from 24 September, when the fraction of *Synechococcus* was largely substituted by *Prochlorococcus*. The dominant groups in the deeper layers shifted toward *Prochlorococcus* (particularly LL subpopulation), prymnesiophytes, and chrysophytes, which collectively comprised > 80% of the TChl *a*.

Environmental factors associated with variations in phytoplankton community structure

To assess temporal differences in phytoplankton community composition, a Bray–Curtis dissimilarity index was applied to data from the upper mixed layer. Both taxa- and pigment-derived Bray–Curtis dissimilarity-based dendrograms showed that the samples across these days could be assigned to two clusters, with the phytoplankton community composition on 24 September clearly distinguished from the remainder (Fig. 4; Supporting Information Fig. S7). In line with the clusters made for Bray–Curtis dissimilarities, the variability of community compositions visualized by PCA exhibited the same separation, with two corresponding clusters (Fig. 5a). Analyses of a range of environmental factors characterizing the community compositions (PCA ordination) across the

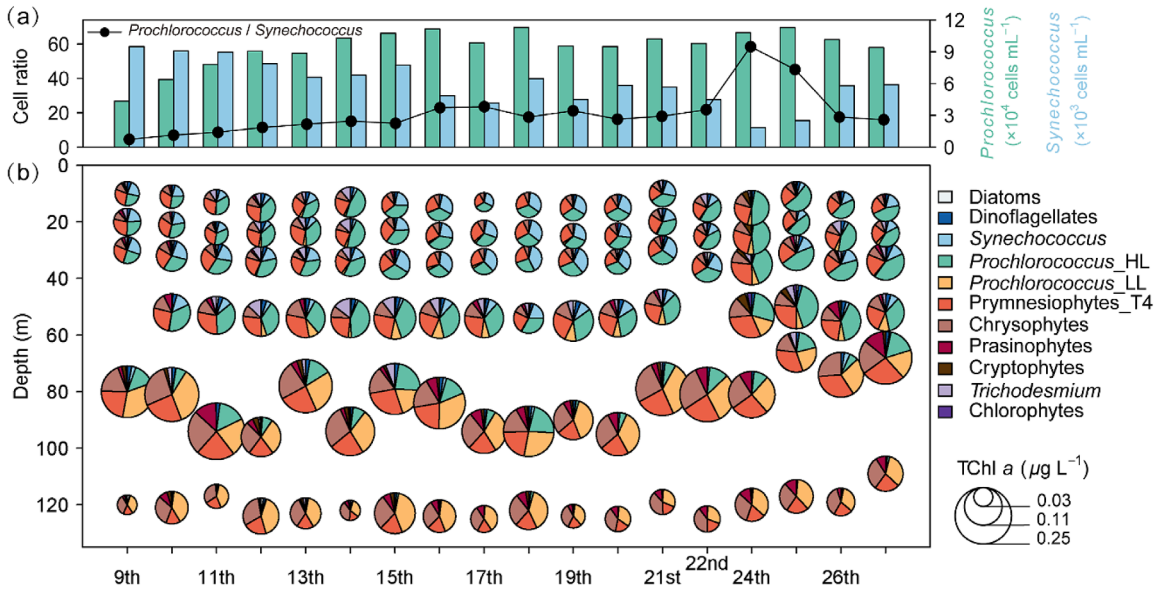

Fig. 3. Phytoplankton community structure. (**a**) Near-surface cell concentrations of *Prochlorococcus* and *Synechococcus* (bars), and their associated cell concentration ratios (line). (**b**) Depth profiles of community composition and biomass (TChl *a*). Pie chart size is proportional to TChl *a*, and composition reflects the pigment-derived taxonomic contributions to TChl *a*.

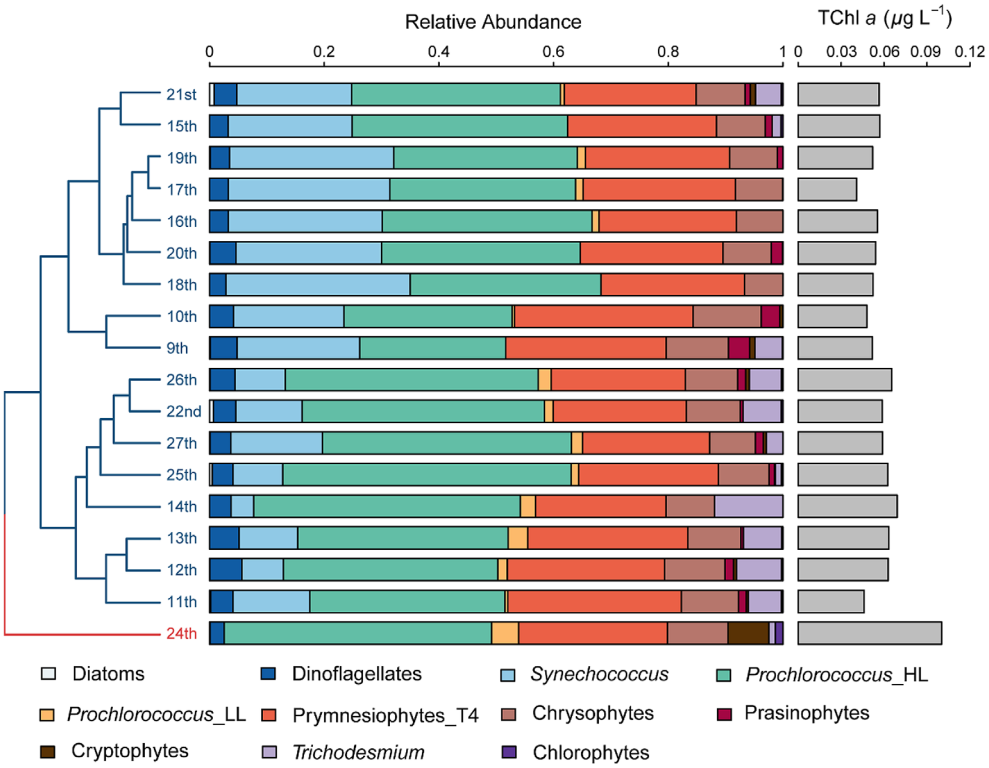

Fig. 4. Bray–Curtis dissimilarity-based dendrogram showing the clustering of pigment-derived taxonomic composition and biomass (TChl *a*) in the mixed layer. Major clusters are indicated by the colors of the branches.

observations demonstrated that precipitation was the most important contributor ($R^2 = 0.76$, $p = 0.046$), followed by DAI ($R^2 = 0.65$, $p = 0.001$), and salinity ($R^2 = 0.55$, $p = 0.001$), while temperature, SLA, nitrate, phosphate, DFe, and DCu were not significantly correlated (Fig. 5b). However, correlations differed among phytoplankton groups when defining

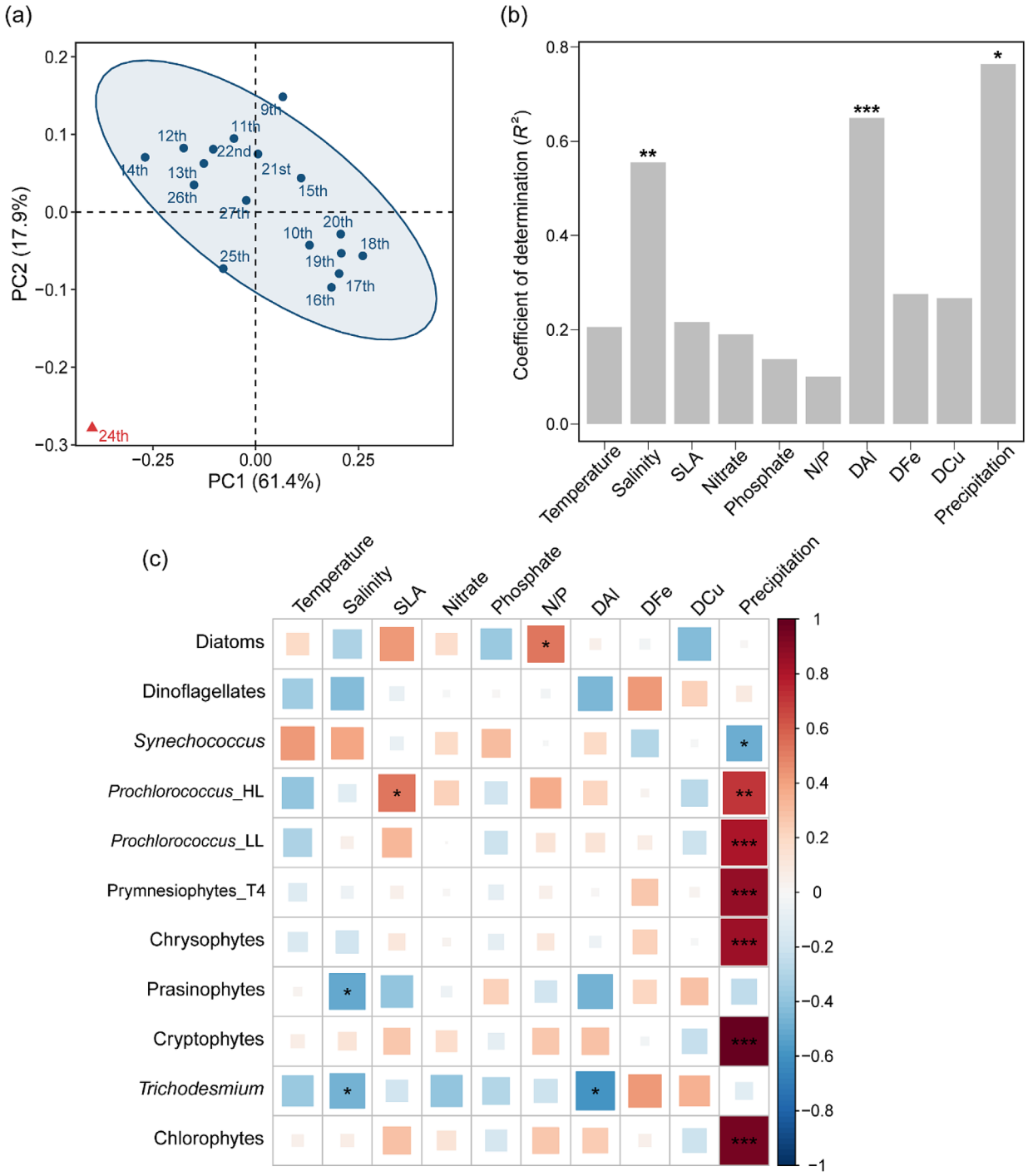

Fig. 5. Ordination and the importance of environmental factors to the pigment-derived community composition in the mixed layer. (**a**) PCA ordination of the phytoplankton community composition with different colors (ellipses) denoting different clusters. Percentages of total variance are explained by PC1 and PC2, accounting for 61.4% and 17.9%, respectively. (**b**) The contribution of environmental factors to the PCA ordination plot, with coefficient of determination (R^2) indicating the contributed proportion. (**c**) Pairwise correlations between environmental factors and phytoplankton groups with a color gradient denoting Pearson's correlation coefficient. Asterisks represent the statistical significance (***$p < 0.001$, **$p < 0.01$, *$p < 0.05$).

environmental factors separately for each group (Fig. 5c). In this case, precipitation was found to be significantly and positively correlated with the dominant *Prochlorococcus* (including both HL and LL subpopulation) and prymnesiophytes fractional contribution to TChl *a*, as well as the less abundant chrysophytes, cryptophytes, and chlorophytes, but significantly

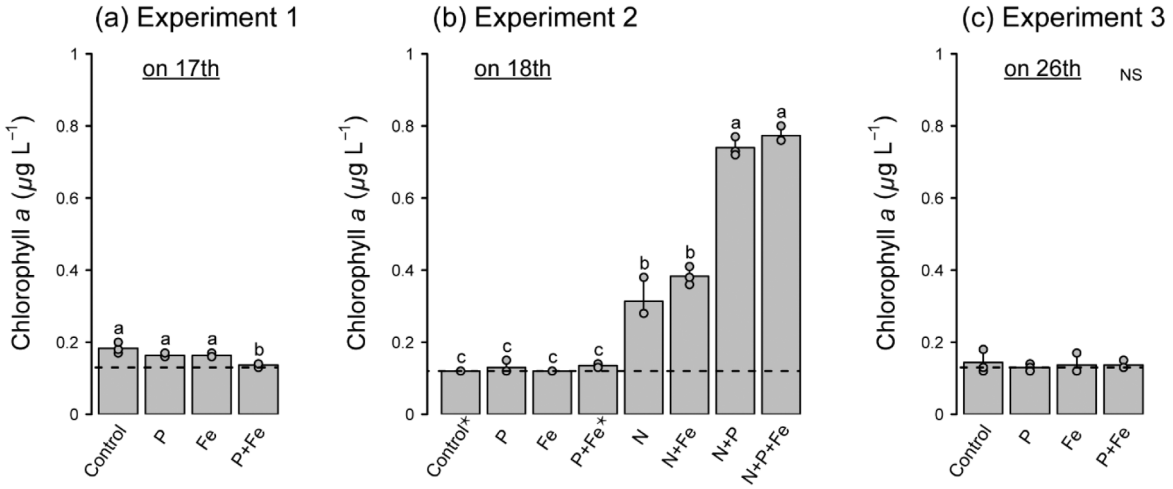

Fig. 6. Chl *a* responses to nutrient additions at the start and end points of experiments. (**a**–**c**) Experiments 1–3. Bars are means of replicates with individual values shown as points, $n = 3$ for all except where indicated by an asterisk ($n = 2$). The horizontal dashed lines indicate initial time measurements. Treatment means are compared using a one-way ANOVA and followed by a post hoc Tukey HSD means comparison test (statistically indistinguishable means are labeled with the same letter, $p < 0.05$; NS is "not significant"). Experiments 1 and 3 were ran for ~ 24 h and Experiment 2 for ~ 50 h.

negatively correlated with the contribution of *Synechococcus* to TChl *a*. No significant correlations with precipitation were found for diatoms, dinoflagellates, prasinophytes, or *Trichodesmium*. In contrast, DAl and salinity were only significantly correlated with prasinophytes (negative correlation with salinity) and *Trichodesmium* (negative correlation with both). None of the concentrations of nitrate, phosphate, DFe, or DCu were significantly correlated with any of the phytoplankton groups.

Phytoplankton responses to nutrient amendment

Two nutrient amendment bioassay experiments (Experiments 1 and 2) were conducted before the episodic rainfall while one (Experiment 3) was conducted after this event (Fig. 6). Collectively, additions of either P or Fe alone or in combination failed to stimulate any significant increase in Chl *a* relative to the controls for any of the experiments. In contrast, the addition of N alone resulted in a 2.6-fold Chl *a* increase over the controls, whereby the supplementary addition of P produced a further Chl *a* increase (6.2-fold over the controls).

Discussion

Nutrient limitation pattern at the study site

The bioassay experiments conducted suggested, (1) primary N limitation of the overall phytoplankton community, with P playing a secondary limiting role (Fig. 6), consistent with the well-established patterns of nutrient limitation in the tropical and subtropical North Atlantic (Moore et al. 2013; Browning et al. 2017); and (2) unresolvable enhancement in Chl *a* associated with any potential P and/or Fe stimulation of N_2 fixation by diazotrophs, which are expected to be limited by P and/or Fe availability (Sañudo-Wilhelmy et al. 2001; Mills et al. 2004; Moore et al. 2009). The lack of enhancement in Chl *a* following P and/or Fe additions in Experiment 3, which was conducted 2 d after the rainfall event, also indicated that the primary N limitation was not fully alleviated by any N supplied by the wet deposition event, consistent with the observation of depleted surface nitrate concentrations.

Phytoplankton stimulated by wet deposition of aerosols

Elevated aerosol deposition fluxes (1.6 mg m^{-2} d^{-1}) derived from DAl concentrations, together with elevated satellite-derived AOT (Supporting Information Fig. S3), were simultaneously present on 17 September, suggestive of a dry deposition event associated with a dust storm. Even higher deposition fluxes were observed on 24 September to 25 September (2.1 and 3.0 mg m^{-2} d^{-1}, respectively), coinciding with a precipitation event (Supporting Information Fig. S4), suggestive of a wet aerosol deposition event. Across the 19-d study period, only on 24 September was there an anomalous increase in phytoplankton biomass and a shift in community composition (Figs. 3, 4; Supporting Information Fig. S6). Our bioassay experiments revealed that N was the proximal limiting nutrient for the overall phytoplankton community at this site (Fig. 6). As no major decrease in loss processes (e.g., grazing) were expected to be associated with the precipitation event, an extra influx of N was thus required to support the observed phytoplankton enhancement. Multiple mechanisms leading to an increase in N supply could potentially be invoked. First, transient upwelling of deeper, N-riched waters to the surface could supply limiting nutrients and fuel-enhanced phytoplankton growth (Wilson 2021); however, the persistently positive SLA suggested overall downwelling of the N-depleted surface waters (Fig. 1b) and the depth profiles of relevant hydrological parameters also showed no evidence of an uplifted isosurface (Fig. 2a–c). Enhanced N supply from greater depths was therefore unlikely. Second, lateral advection and mixing of waters from elsewhere could potentially

supply N, but this is also considered unlikely due to the consistency of N-depleted surface waters throughout the region (Fig. 2d). Finally, this could have been driven by wet aerosol deposition associated with the rainfall event. This could have, in turn, occurred via two mechanisms. First, wet deposition likely enhanced the supply rate of DFe (Fig. 2g; Buck et al. 2006; Baker et al. 2013; Schlosser et al. 2014), which might have stimulated N_2 fixation activity and therefore increased supply of bioavailable N into the system (Schlosser et al. 2014). However, supply of DFe and/or phosphate in the bioassay incubation experiments led to no such increase in Chl *a* over 2 d of incubation (Fig. 6), which was longer than the natural response time of in situ Chl *a* to the rainfall event (Fig. 1c). This therefore suggested that any enhancement in N_2 fixation activity was either too slow or too low in magnitude to drive the observed Chl *a* enhancement. This thus points towards a direct increase in aerosol N supply due to the episodic rainfall as the predominant driving mechanism behind the observed phytoplankton enhancement. This mechanism is further reinforced by our envfit analysis and pairwise comparisons, which indicate precipitation to be the primary controlling factor in shaping the unique community composition on 24 September relative to the other days (Fig. 5b,c).

We calculated the approximate amount of N required to support the observed increase in Chl *a* (determined as the difference between enhancement and pre-enhancement) within the MLD (26 m), assuming an average Chl *a*-to-carbon ratio of 0.02 (by weight; Behrenfeld et al. 2005) and a carbon-to-nitrogen molar ratio of 6.6 in phytoplankton elemental stoichiometry (Redfield et al. 1963). We found that the required N flux was 1.48 mmol m^{-2} d^{-1}. Based on a precipitation rate of 61 mm d^{-1} (Fig. 1c), we then estimated the required N concentration in rainwater to be approximately 24.2 μmol L^{-1}. Acknowledging high levels of uncertainty in our calculation, this value was generally consistent with, but on the higher end of, previously observed rainwater nitrate plus ammonium concentration around this region (30–40°W, 30–40°N) with the range of 1.8–24.7 μmol L^{-1} (https://www.bodc.ac.uk/solas_integration/implementation_products/group1/aerosol_rain/).

The most striking shift in community composition associated with the rainfall event was an increase in both cell number and biomass of *Prochlorococcus* (HL subpopulation) at the expense of *Synechococcus* (Figs. 3, 4). Several mechanisms can be hypothesized to have driven this community shift. First, *Prochlorococcus*, the smallest phytoplankton with a diameter of 0.5–0.7 μm, has been reported to have relatively lower P requirements and is capable of efficient P utilization (Heldal et al. 2003; Van Mooy et al. 2006; Martiny et al. 2009), potentially allowing them to outcompete *Synechococcus* when exposed to aerosols with high N: P ratios. This generally matched well with a previous modeling study, which suggested that high cellular N : P ratios of *Prochlorococcus* (25 : 1), compared to *Synechococcus* (21 : 1), enabled them to become more competitive, especially in the high aerosol loading portion of the NASG (Chien et al. 2016). Although we did not measure the chemical compositions of aerosols in this study, previous measurements have shown that the ratios of N : P in the soluble fraction of aerosols (~ 500–5000) were far higher than the ratio typically required by phytoplankton of 16N : 1P (Baker et al. 2010; Zamora et al. 2013). Second, the likely high proportion of ammonium and soluble organic nitrogen compared to nitrate in these aerosols, for example, accounting for over 50% of total aerosol N at Bermuda (Altieri et al. 2016), may have further benefited the predominance of *Prochlorococcus* over *Synechococcus* (García-Fernández et al. 2004). Finally, the potentially elevated concentrations of other trace elements, such as DCu, could potentially suppress *Synechococcus*, whereas the HL subpopulation of *Prochlorococcus* is known to be more resistant to copper toxicity (Mann et al. 2002; Paytan et al. 2009). Arguing against the latter were the measured surface DCu concentrations, which were 0.86 nmol L^{-1} during the rainfall event in comparison to higher average background concentrations of 1.35 ± 0.47 nmol L^{-1} (although noting that DCu speciation might be important in regulating toxicity; Mackey et al. 2012). In addition to the increase in *Prochlorococcus*, the modest 3–27% estimated increase in the Chl *a* biomass of larger phytoplankton groups including prymnesiophytes, cryptophytes, chrysophytes, and chlorophytes could also be associated with enhanced N supply from wet aerosol deposition. No detected stimulation of even larger phytoplankton groups (diatoms, dinoflagellates) could be explained by their initially very low biomass (Supporting Information Fig. S6).

Contrasting phytoplankton responses between wet and dry deposition

Despite the dust storm (dry deposition) being calculated to have a similar aerosol deposition flux as the wet deposition event (1.6 and 2.6 mg m^{-2} d^{-1}, respectively and noting uncertainties associated in their calculation), it contrasted with the wet deposition event in not matching up with any observable change in phytoplankton biomass or community composition. We hypothesize that this discrepancy in biological response could be attributed to two factors. First, it could be due to the varying N content and bioavailability in aerosols of different origins, which can have divergent physicochemical compositions and different atmospheric processing (Mackey et al. 2012; Guieu et al. 2014). Specifically, within our field observation period, air mass back-trajectories indicated that the air over our study location mostly originated from North America and the open ocean, with the exception of those on 23 September, 24 September, and 27 September, which had previously traversed North Africa and southern Europe (Fig. 7). The latter source likely entrained more bioavailable nutrients due to the reported higher N loading from the Saharan dust and industrialized regions of Europe (Baker et al. 2010; Baker and Jickells 2017), as well as a shorter transport distance, a factor known to control the magnitude of deposition flux (Lawrence and Neff 2009). Second, the subsequent deposition pathway (dry or wet deposition) may further

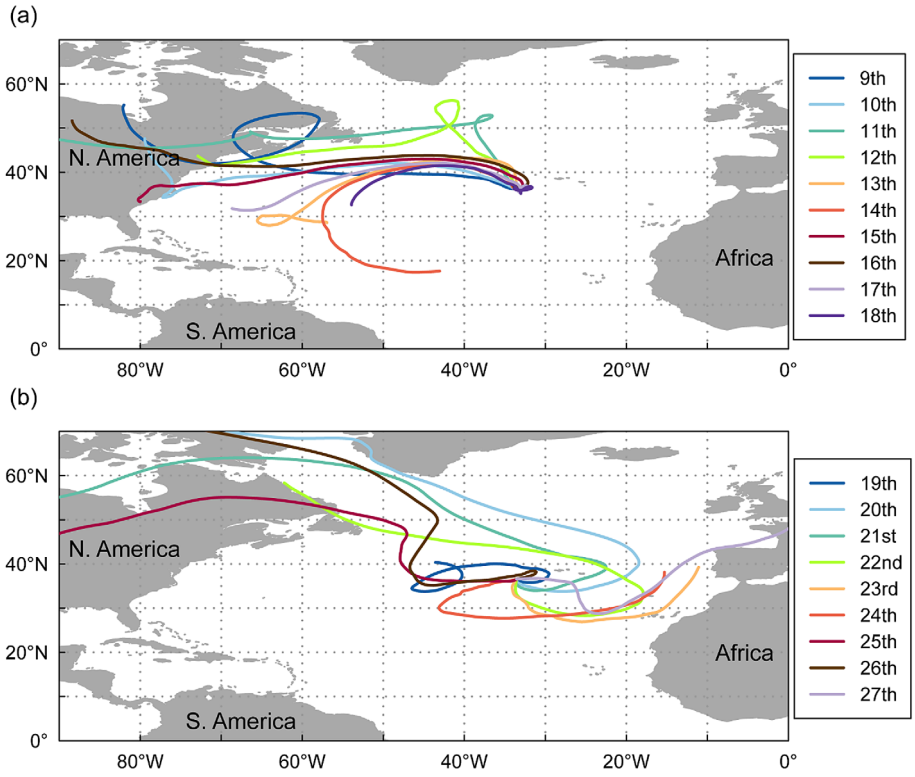

Fig. 7. Representative 7-d air mass backward trajectories calculated for (**a**) 09 September 2021 to 18 September 2021, and (**b**) 19 September 2021 to 27 September 2021.

determine the amounts of accessible N for phytoplankton in the receiving seawaters. In the wet deposition scenario, rainwater can enrich more N into aerosols via mixing with nitric acid (Meskhidze et al. 2003; Guieu et al. 2010), as well as introducing zero-salinity rainwaters driving enhanced stratification of the near surface water (Fig. 2b), thereby, retaining N-rich rainwaters in the surface ocean for a longer period.

Conclusions

Using 19 d of field observations at a site in the subtropical North Atlantic, we find contrasting phytoplankton responses between dry and wet aerosol deposition events: the wet deposition event led to a rapid accumulation of phytoplankton and a shift in phytoplankton community toward a greater contribution of *Prochlorococcus* at the expense of *Synechococcus*, while the dry deposition event did not lead to any observable phytoplankton response. We attribute these differences in responses to both the wet or dry deposition pathways as well as the aerosol source locations (Sahara Desert and Continental Europe for the wet deposition event, North America and open ocean for the dry deposition event) resulting in different supply rates of bioavailable N to seawater. Our findings underscore the importance of both deposition mode and source location in regulating phytoplankton responses, for example, when evaluating the impact of aerosol N input in biogeochemical model simulations (Krishnamurthy et al. 2007; Jickells et al. 2017). This is particularly pertinent given that projected warming and stratification of the upper ocean (Fu et al. 2016), alongside increased aerosol N deposition (Jickells et al. 2017) and extreme rainfall frequencies (Westra et al. 2014) are expected to increase the importance of aerosol fertilization of the low latitude oceans. Alongside other factors (Flombaum et al. 2013), our results also suggest that such changes may furthermore contribute to regulating the relative abundance of *Prochlorococcus* over *Synechococcus* in the low-latitude subtropical oceans.

Data availability statement

Data are stored and available on Zenodo via the doi: 10.5281/zenodo.7989871.

References

Albani, S., and others. 2014. Improved dust representation in the community atmosphere model. J. Adv. Model. Earth Syst. **6**: 541–570. doi:10.1002/2013MS000279

Altieri, K. E., S. E. Fawcett, A. J. Peters, D. M. Sigman, and M. G. Hastings. 2016. Marine biogenic source of atmospheric organic nitrogen in the subtropical North Atlantic.

Proc. Natl. Acad. Sci. U.S.A. **113**: 925–930. doi:10.1073/pnas.1516847113

Ardyna, M., and others. 2022. Wildfire aerosol deposition likely amplified a summertime Arctic phytoplankton bloom. Commun. Earth Environ. **3**: 1–8. doi:10.1038/s43247-022-00511-9

Baker, A. R., T. D. Jickells, K. F. Biswas, K. Weston, and M. French. 2006. Nutrients in atmospheric aerosol particles along the Atlantic Meridional Transect. Deep Sea Res. Res. II Topic. Stud. Oceonogr. **53**: 1706–1719. doi:10.1016/j.dsr2.2006.05.012

Baker, A. R., K. Weston, S. D. Kelly, M. Voss, P. Streu, and J. N. Cape. 2007. Dry and wet deposition of nutrients from the tropical Atlantic atmosphere: Links to primary productivity and nitrogen fixation. Deep Sea Res. I Oceanogr. Res. Pap. **54**: 1704–1720. doi:10.1016/j.dsr.2007.07.001

Baker, A. R., T. Lesworth, C. Adams, T. D. Jickells, and L. Ganzeveld. 2010. Estimation of atmospheric nutrient inputs to the Atlantic Ocean from 50°N to 50°S based on large-scale field sampling: Fixed nitrogen and dry deposition of phosphorus. Global Biogeochem. Cycl. **24**: GB3006. doi:10.1029/2009GB003634

Baker, A. R., C. Adams, T. G. Bell, T. D. Jickells, and L. Ganzeveld. 2013. Estimation of atmospheric nutrient inputs to the Atlantic Ocean from 50°N to 50°S based on large-scale field sampling: Iron and other dust-associated elements. Global Biogeochem. Cycl. **27**: 755–767. doi:10.1002/gbc.20062

Baker, A. R., and T. D. Jickells. 2017. Atmospheric deposition of soluble trace elements along the Atlantic Meridional Transect (AMT). Prog. Oceanogr. **158**: 41–51. doi:10.1016/j.pocean.2016.10.002

Barraqueta, J. L. M., and others. 2019. Atmospheric deposition fluxes over the Atlantic Ocean: A GEOTRACES case study. Biogeosciences **16**: 1525–1542. doi:10.5194/bg-16-1525-2019

Behrenfeld, M. J., E. Boss, D. A. Siegel, and D. M. Shea. 2005. Carbon-based ocean productivity and phytoplankton physiology from space. Global Biogeochem. Cycl. **19**: 1–14. doi:10.1029/2004GB002299

Benaltabet, T., G. Lapid, and A. Torfstein. 2022. Dissolved aluminium dynamics in response to dust storms, wet deposition, and sediment resuspension in the Gulf of Aqaba, northern Red Sea. Geochim. Cosmochim. Acta **335**: 137–154. doi:10.1016/j.gca.2022.08.029

Bishop, J. K. B., R. E. Davis, and J. T. Sherman. 2002. Robotic observations of dust storm enhancement of carbon biomass in the North Pacific. Science **298**: 817–821. doi:10.1126/science.1074961

Boyd, P. W., D. S. Mackie, and K. A. Hunter. 2010. Aerosol iron deposition to the surface ocean—Modes of iron supply and biological responses. Mar. Chem. **120**: 128–143. doi:10.1016/j.marchem.2009.01.008

Browning, T. J., E. P. Achterberg, I. Rapp, A. Engel, E. M. Bertrand, A. Tagliabue, and C. M. Moore. 2017. Nutrient co-limitation at the boundary of an oceanic gyre. Nature **551**: 242–246. doi:10.1038/nature24063

Buck, C. S., W. M. Landing, J. A. Resing, and G. T. Lebon. 2006. Aerosol iron and aluminum solubility in the northwest Pacific Ocean: Results from the 2002 IOC cruise. Geochem. Geophys. Geosyst. **7**: 4–7. doi:10.1029/2005GC000977

Chien, C. T., K. R. M. Mackey, S. Dutkiewicz, N. M. Mahowald, J. M. Prospero, and A. Paytan. 2016. Effects of African dust deposition on phytoplankton in the western tropical Atlantic Ocean off Barbados. Global Biogeochem. Cycl. **30**: 716–734. doi:10.1002/2015GB005334

de Boyer Montégut, C., G. Madec, A. S. Fischer, A. Lazar, and D. Iudicone. 2004. Mixed layer depth over the global ocean: An examination of profile data and a profile-based climatology. J. Geophys. Res. Oceans **109**: 1–20. doi:10.1029/2004JC002378

DiTullio, G. R., and E. A. Laws. 1991. Impact of an atmospheric-oceanic disturbance on phytoplankton community dynamics in the North Pacific Central Gyre. Deep Sea Res. A Oceanogr. Res. Pap. **38**: 1305–1329. doi:10.1016/0198-0149(91)90029-F

Duce, R. A., and others. 1991. The atmospheric input of trace species to the world ocean. Global Biogeochem. Cycl. **5**: 193–259. doi:10.1029/91GB01778

Emerson, S., P. Quay, D. Karl, C. Winn, L. Tupas, and M. Landry. 1997. Experimental determination of the organic carbon flux from open-ocean surface waters. Nature **389**: 951–954. doi:10.1038/40111

Flombaum, P., and others. 2013. Present and future global distributions of the marine cyanobacteria *Prochlorococcus* and *Synechococcus*. Proc. Natl. Acad. Sci. U.S.A. **110**: 9824–9829. doi:10.1073/PNAS.1307701110/-/DCSUPPLEMENTAL

Fu, W., J. T. Randerson, and J. Keith Moore. 2016. Climate change impacts on net primary production (NPP) and export production (EP) regulated by increasing stratification and phytoplankton community structure in the CMIP5 models. Biogeosciences **13**: 5151–5170. doi:10.5194/bg-13-5151-2016

García-Fernández, J. M., N. T. de Marsac, and J. Diez. 2004. Streamlined regulation and gene loss as adaptive mechanisms in *Prochlorococcus* for optimized nitrogen utilization in oligotrophic environments. Microbiol. Mol. Biol. Rev. **68**: 630–638. doi:10.1128/mmbr.68.4.630-638.2004

Guieu, C., and others. 2010. Large clean mesocosms and simulated dust deposition: A new methodology to investigate responses of marine oligotrophic ecosystems to atmospheric inputs. Biogeosciences **7**: 2765–2784. doi:10.5194/bg-7-2765-2010

Guieu, C., and others. 2014. The significance of the episodic nature of atmospheric deposition to low nutrient low chlorophyll regions. Global Biogeochem. Cycl. **28**: 1179–1198. doi:10.1002/2014GB004852

Hamilton, D. S., and others. 2022. Earth, wind, fire, and pollution: Aerosol nutrient sources and impacts on ocean biogeochemistry. Ann. Rev. Mar. Sci. **14**: 303–330. doi:10.1146/annurev-marine-031921-013612

Han, Q., J. K. Moore, C. Zender, C. Measures, and D. Hydes. 2008. Constraining oceanic dust deposition using surface ocean dissolved Al. Global Biogeochem. Cycl. **22**: 1–14. doi:10.1029/2007GB002975

Heldal, M., D. J. Scanlan, S. Norland, F. Thingstad, and N. H. Mann. 2003. Elemental composition of single cells of various strains of marine *Prochlorococcus* and *Synechococcus* using X-ray microanalysis. Limnol. Oceanogr. **48**: 1732–1743. doi:10.4319/lo.2003.48.5.1732

Jickells, T., and C. M. Moore. 2015. The importance of atmospheric deposition for ocean productivity. Annu. Rev. Ecol. Evol. Syst. **46**: 481–501. doi:10.1146/annurev-ecolsys-112414-054118

Jickells, T. D., and others. 2017. A reevaluation of the magnitude and impacts of anthropogenic atmospheric nitrogen inputs on the ocean. Global Biogeochem. Cycl. **31**: 289–305. doi:10.1002/2016GB005586

Jung, J., H. Furutani, and M. Uematsu. 2011. Atmospheric inorganic nitrogen in marine aerosol and precipitation and its deposition to the North and South Pacific Oceans. J. Atmos. Chem. **68**: 157–181. doi:10.1007/s10874-012-9218-5

Kramer, S. J., K. M. Bisson, and A. D. Fischer. 2020. Observations of phytoplankton community composition in the Santa Barbara Channel during the Thomas fire. J. Geophys. Res. Oceans **125**: e2020JC016851. doi:10.1029/2020JC016851

Krishnamurthy, A., J. K. Moore, C. S. Zender, and C. Luo. 2007. Effects of atmospheric inorganic nitrogen deposition on ocean biogeochemistry. J. Geophys. Res. Biogeo. **112**: 2019. doi:10.1029/2006JG000334

Lawrence, C. R., and J. C. Neff. 2009. The contemporary physical and chemical flux of aeolian dust: A synthesis of direct measurements of dust deposition. Chem. Geol. **267**: 46–63. doi:10.1016/j.chemgeo.2009.02.005

Leblanc, K., and others. 2018. Nanoplanktonic diatoms are globally overlooked but play a role in spring blooms and carbon export. Nat. Commun. **9**: 1–12. doi:10.1038/s41467-018-03376-9

Mackey, M. D., D. J. Mackey, H. W. Higgins, and S. W. Wright. 1996. CHEMTAX—A program for estimating class abundances from chemical markers: Application to HPLC measurements of phytoplankton. Mar. Ecol. Prog. Ser. **144**: 265–283. doi:10.3354/MEPS144265

Mackey, K. R. M., K. N. Buck, J. R. Casey, A. Cid, M. W. Lomas, Y. Sohrin, and A. Paytan. 2012. Phytoplankton responses to atmospheric metal deposition in the coastal and open-ocean Sargasso Sea. Front. Microbiol. **3**: 359. doi:10.3389/fmicb.2012.00359

Mahadevan, A., E. D'Asaro, C. Lee, and M. J. Perry. 2012. Eddy-driven stratification initiates North Atlantic spring phytoplankton blooms. Science **336**: 54–58. doi:10.1126/science.1218740

Mann, E. L., N. Ahlgren, J. W. Moffett, and S. W. Chisholm. 2002. Copper toxicity and cyanobacteria ecology in the Sargasso Sea. Limnol. Oceanogr. **47**: 976–988. doi:10.4319/lo.2002.47.4.0976

Marañón, E. 2005. Phytoplankton growth rates in the Atlantic subtropical gyres. Limnol. Oceanogr. **50**: 299–310. doi:10.4319/lo.2005.50.1.0299

Martin, P., R. S. Lampitt, M. Jane Perry, R. Sanders, C. Lee, and E. D'Asaro. 2011. Export and mesopelagic particle flux during a North Atlantic spring diatom bloom. Deep. Res. Res. I Oceanogr. Res. Pap. **58**: 338–349. doi:10.1016/j.dsr.2011.01.006

Martino, M., D. Hamilton, A. R. Baker, T. D. Jickells, T. Bromley, Y. Nojiri, B. Quack, and P. W. Boyd. 2014. Western Pacific atmospheric nutrient deposition fluxes, their impact on surface ocean productivity. Global Biogeochem. Cycl. **28**: 712–728. doi:10.1002/2013GB004794

Martiny, A. C., Y. Huang, and W. Li. 2009. Occurrence of phosphate acquisition genes in Prochlorococcus cells from different ocean regions. Environ. Microbiol. **11**: 1340–1347. doi:10.1111/j.1462-2920.2009.01860.x

Measures, C. I., and E. T. Brown. 1996. Estimating dust input to the Atlantic Ocean using surface water aluminium concentrations, p. 301–311. *In* S. Guerzoni and R. Chester [eds.], The impact of desert dust across the Mediterranean. Springer.

Meskhidze, N., W. L. Chameides, A. Nenes, and G. Chen. 2003. Iron mobilization in mineral dust: Can anthropogenic SO_2 emissions affect ocean productivity? Geophys. Res. Lett. **30**: 2085. doi:10.1029/2003gl018035

Middag, R., M. M. P. van Hulten, H. M. Van Aken, M. J. A. Rijkenberg, L. J. A. Gerringa, P. Laan, and H. J. W. de Baar. 2015. Dissolved aluminium in the ocean conveyor of the West Atlantic Ocean: Effects of the biological cycle, scavenging, sediment resuspension and hydrography. Mar. Chem. **177**: 69–86. doi:10.1016/j.marchem.2015.02.015

Mignot, A., R. Ferrari, and H. Claustre. 2018. Floats with bio-optical sensors reveal what processes trigger the North Atlantic bloom. Nat. Commun. **9**: 1–9. doi:10.1038/s41467-017-02143-6

Milinković, A., and others. 2022. Variabilities of biochemical properties of the sea surface microlayer: Insights to the atmospheric deposition impacts. Sci. Total Environ. **838**: 156440. doi:10.1016/j.scitotenv.2022.156440

Mills, M. M., C. Ridame, M. Davey, J. La Roche, and R. J. Geider. 2004. Iron and phosphorus co-limit nitrogen fixation in the eastern tropical North Atlantic. Nature **429**: 292–294. doi:10.1038/nature02550

Moore, C. M., and others. 2009. Large-scale distribution of Atlantic nitrogen fixation controlled by iron availability. Nat. Geosci. **2**: 867–871. doi:10.1038/ngeo667

Moore, C. M., and others. 2013. Processes and patterns of oceanic nutrient limitation. Nat. Geosci. **6**: 701–710. doi:10.1038/ngeo1765

Moran, S. B., and R. M. Moore. 1988. Evidence from mesocosm studies for biological removal of dissolved aluminium from sea water. Nature **335**: 706–708. doi:10.1038/335706a0

Oksanen, J., and others. 2022. vegan: Community ecology package. R package version 2.6-2. https://CRAN.R-project.org/package=vegan

Patey, M. D., M. J. A. Rijkenberg, P. J. Statham, M. C. Stinchcombe, E. P. Achterberg, and M. Mowlem. 2008. Determination of nitrate and phosphate in seawater at nanomolar concentrations. Trends Anal. Chem. **27**: 169–182. doi:10.1016/j.trac.2007.12.006

Patey, M. D., E. P. Achterberg, M. J. Rijkenberg, and R. Pearce. 2015. Aerosol time-series measurements over the tropical Northeast Atlantic Ocean: Dust sources, elemental composition and mineralogy. Mar. Chem. **174**: 103–119. doi:10.1016/j.marchem.2015.06.004

Paytan, A., K. R. M. Mackey, Y. Chen, I. D. Lima, S. C. Doney, N. Mahowald, R. Labiosa, and A. F. Post. 2009. Toxicity of atmospheric aerosols on marine phytoplankton. Proc. Natl. Acad. Sci. U.S.A. **106**: 4601–4605. doi:10.1073/PNAS.0811486106

R Development Core Team. 2021. R: A language and environment for statistical computing. R Foundation for Statistical Computing.

Rapp, I., C. Schlosser, D. Rusiecka, M. Gledhill, and E. P. Achterberg. 2017. Automated preconcentration of Fe, Zn, Cu, Ni, Cd, Pb, Co, and Mn in seawater with analysis using high-resolution sector field inductively-coupled plasma mass spectrometry. Anal. Chim. Acta **976**: 1–13. doi:10.1016/J.ACA.2017.05.008

Redfield, A. C., B. H. Ketchum, and F. A. Richards. 1963. The influence of organisms on the composition of seawater. Sea **2**: 26–77.

Ren, J. L., J. Zhang, J. Q. Luo, X. K. Pei, and Z. X. Jiang. 2001. Improved fluorimetric determination of dissolved aluminium by micelle-enhanced lumogallion complex in natural waters. Analyst **126**: 698–702. doi:10.1039/b007593k

Ridame, C., J. Dekaezemacker, C. Guieu, S. Bonnet, S. L'Helguen, and F. Malien. 2014. Contrasted Saharan dust events in LNLC environments: Impact on nutrient dynamics and primary production. Biogeosciences **11**: 4783–4800. doi:10.5194/bg-11-4783-2014

Sañudo-Wilhelmy, S. A., and others. 2001. Phosphorus limitation of nitrogen fixation by Trichodesmium in the central Atlantic Ocean. Nature **411**: 66–69. doi:10.1038/35075041

Schlosser, C., and others. 2014. Seasonal ITCZ migration dynamically controls the location of the (sub)tropical Atlantic biogeochemical divide. Proc. Natl. Acad. Sci. U.S.A. **111**: 1438–1442. doi:10.1073/pnas.1318670111

Talley, L. D., G. L. Pickard, W. J. Emery, and J. H. Swift. 2011. Descriptive physical oceanography: An introduction. Academic Press.

Tang, W., and others. 2021. Widespread phytoplankton blooms triggered by 2019–2020 Australian wildfires. Nature **597**: 370–375. doi:10.1038/s41586-021-03805-8

Van Heukelem, L., and C. S. Thomas. 2001. Computer-assisted high-performance liquid chromatography method development with applications to the isolation and analysis of phytoplankton pigments. J. Chromatogr. A **910**: 31–49. doi:10.1016/S0378-4347(00)00603-4

Van Mooy, B. A. S., G. Rocap, H. F. Fredricks, C. T. Evans, and A. H. Devol. 2006. Sulfolipids dramatically decrease phosphorus demand by picocyanobacteria in oligotrophic marine environments. Proc. Natl. Acad. Sci. U.S.A. **103**: 8607–8612. doi:10.1073/pnas.0600540103

Van Wambeke, F., and others. 2021. Influence of atmospheric deposition on biogeochemical cycles in an oligotrophic ocean system. Biogeosciences **18**: 5699–5717. doi:10.5194/bg-18-5699-2021

Veldhuis, M. J. W., and G. W. Kraay. 2004. Phytoplankton in the subtropical Atlantic Ocean: Towards a better assessment of biomass and composition. Deep Sea Res. I Oceanogr. Pap. **51**: 507–530. doi:10.1016/j.dsr.2003.12.002

Welschmeyer, N. A. 1994. Fluorometric analysis of chlorophyll *a* in the presence of chlorophyll b and pheopigments. Limnol. Oceanogr. **39**: 1985–1992. doi:10.4319/LO.1994.39.8.1985

Westra, S., and others. 2014. Future changes to the intensity and frequency of short-duration extreme rainfall. Rev. Geophys. **52**: 522–555. doi:10.1002/2014RG000464

Wilson, C. 2021. Evidence of episodic nitrate injections in the oligotrophic North Pacific associated with surface chlorophyll blooms. J. Geophys. Res. Oceans **126**: e2021JC017169. doi:10.1029/2021JC017169

Xu, H., and T. Weber. 2021. Ocean dust deposition rates constrained in a data-assimilation model of the marine aluminum cycle. Global Biogeochem. Cycl. **35**: e2021GB007049. doi:10.1029/2021GB007049

Yuan, Z., and others. 2023. Potential drivers and consequences of regional phosphate depletion in the western subtropical North Pacific. Limnol. Oceanogr. Lett. **8**: 509–518. doi:10.1002/lol2.10314

Zamora, L. M., J. M. Prospero, D. A. Hansell, and J. M. Trapp. 2013. Atmospheric P deposition to the subtropical North Atlantic: Sources, properties, and relationship to N deposition. J. Geophys. Res. Atmos. **118**: 1546–1562. doi:10.1002/jgrd.50187

Acknowledgments

The authors thank the captain, crew, and scientists of the RV Meteor M176/2 cruise. Tania Klüver is thanked for assistance with the flow cytometry analysis. Kerstin Nachtigall is thanked for assistance with the HPLC analysis. André Mutzberg is thanked for the nutrient analysis. Tim Steffens and Dominik Jasinski are thanked for assistance with the trace element analysis. Martha Gledhill is thanked for assistance with the analysis of DAl. The research cruise was funded by Deutsche Forschungsgemeinschaft (DFG) grant "RainbowPlume" to EPA and TJB. ZY was supported by the Chinese Scholarship Council (File No. 202106310003). LZ was supported by the Chinese Scholarship Council (File No. 202004910004) and the Development Fund of South China Sea Institute of Oceanology of the Chinese

Academy of Sciences (SCSIO202204). XZ was supported by the Sino-German (CSC-DAAD) Postdoc Scholarship Program (File No. 201806140311). Open Access funding enabled and organized by Projekt DEAL.

Conflict of Interest

None declared.

Submitted 11 April 2023
Revised 07 June 2023
Accepted 16 July 2023

Associate editor: C. Elisa Schaum